engineering proceedings

MDPI

Proceeding Paper

On Maximum Tolerable Multipath for Successful Meta-signal Subcarrier Ambiguity Fixing†

Mohamed Bochkati [1], Ece Kayacilar [1], Muhammad S. Hameed [1] , Markel Arizabaleta-Diez [1] and Thomas Pany [1]

[1] University of the Bundeswehr Munich, 85579 Neubiberg, Germany
* Correspondence: mohamed.bochkati@unibw.de
† Presented at the European Navigation Conference 2024, Noordwijk, The Netherlands, 22–24 May 2024

Abstract: The prospect of GNSS meta-signal tracking promises the synergy of both code reliability and the high-precision of sub-carrier observations. The latter has the advantage, in comparison to carrier-phase observations, of having wavelengths in the order of a few meters instead of cm-level. This realizes the possibility of resolving sub-carrier-phase ambiguities without the need of a reference station providing positioning solutions with a sub-meter level accuracy. In the frame of the HANDS-CD project led by IGASPIN GmbH, a synthetic meta-signal observation formed from Galileo E5a and E5b signals using the widelaning concept will be demonstrated in this contribution. This analysis is performed based on a simulated kinematic trajectory. The synthetic meta-signal observations are fed into an extended Kalman filter-based positioning engine, called meta-signal positioning engine (M-SiPE-tool) which applies the least-squares ambiguity decorrelation adjustment (LAMBDA) ambiguity fixing method to resolve the sub-carrier ambiguities. To assess the robustness of the positioning filter against signal impairments, the observations of many Galileo satellites are synthetically contaminated by multipath reflection with different amplitudes. The outcome of the positioning engine exhibits successful **sub-carrier ambiguity fixing** and provides a sub-decimeter **positioning accuracy** for a code multipath amplitude of less than 30 meters, or for sub-carrier multipath amplitude of less than 0.5 meters.

Keywords: Meta-signal; Sub-carrier-Ambiguity; Multipath

1. Introduction

The need for more robust signals for positioning in harsh environments such as urban canyons, has become increasingly important over the last decades. Low-cost global navigation satellite system (GNSS) chips are nowadays present in smartphones, progressively with more than one frequency, enabling high-accuracy positioning, especially when carrier-phase observations are available and utilized properly. This is attractive for applications such autonomous driving, location-based service (LBS) or even for cost-efficient unmanned aerial vehicles (UAVs), which require robustness due to receiver dynamics as well as when signal interference such as signal jamming is present. Without the need for complementary sensors such inertial measurement unit (IMU) or vision sensors, combining two signal components and processing them as a single entity yield a more accurate and robust signal that benefits from both code-robustness and carrier-phase accuracy. Such type of technique is called meta-signal.

A large variety of techniques exists to process meta-signals, including wideband processing or using dedicated sub-carrier loops. As an important milestone, [1] and [2] have shown that sub-carrier-phase observations are under certain assumptions equivalent to the wide-lane linear combination of the carrier-phase measurements obtained from the two original side-band components. This means meta-signal is equivalent to the wide-lane linear combination of the carrier-phase measurements obtained from two

Citation: To be added by editorial staff during production.

Academic Editor: Firstname Lastname

Published: date

Copyright: © 2024 by the authors. Submitted for possible open access publication under the terms and conditions of the Creative Commons Attribution (CC BY) license (https://creativecommons.org/licenses/by/4.0/).

independently processed signals. Taking these findings into account, it is possible to emulate meta-signal processing by using the wide-lane technique. Therefore, the potential of such signal can be explored directly on the observation level while avoiding the high-complex signal processing stage in the GNSS receiver. Nevertheless, the focus in [1] and [2] was dedicated more for the signal processing side, where the positioning performance was evaluated by a simple single point positioning (SPP) in static case under optimal signal conditions. That means that the challenge faced by the (sub-)carrier observations such as multipath or other signal impairments were not taken into consideration as (sub-)carrier measurements were not used by the positioning engine. This means that the effects of the (sub-)carrier cycle slips have not yet being studied, and therefore, the ambiguity resolution performance in meta-signals have not been analyzed. The most reliable technique for the carrier-phase ambiguity resolution is the LAMBDA-method [3], which we adapt in this contribution to solve the sub-carrier ambiguities (as already demonstrated for the first time in [4]) for different situations, i.e. static and kinematic, with/without signal impairments. Here, the focus will be only on the Galileo E5a-E5b observations, which can be made available by the receiver independent exchange format (RINEX) from any GNSS-receiver/antenna combination which allow the receptions of those signals.

This paper is structured as follows: First, the concept of meta-signal tracking and the derivation of the observables employed for positioning is briefly introduced. In the second section, an overview about our extended Kalman filter (EKF)-based positioning engine, M-SiPE-tool, which processes both the meta-signal pseudorange and sub-carrier observation, will be given. Afterwards, the performance of this engine for various multipath scenarios will be presented and analyzed, based on a simulated kinematic car trajectory. The last section concludes the paper by providing a short summary and conclusions.

2. Generation of Meta-Signal Observables

The generated meta-signal observations correspond to the E5a-E5b meta-signal as described in [1] by using the narrow- and wide-lane techniques. These techniques employ the pseudorange and carrier-phase information of the narrowband processing output of the Galileo E5a and E5b signals, to generate the meta-signal carrier-phase, meta-signal sub-carrier-phase, and meta-signal pseudorange observations.

The meta-signal carrier-phase observation, φ_0, is computed by applying the narrow-lane carrier-phase combination of the processed side-band carrier-phase observations, i.e.

$$\varphi_0 = \left(\frac{\Phi_1}{\lambda_1} + \frac{\Phi_2}{\lambda_2}\right) \quad (1)$$

where Φ_i and λ_i are the carrier-phase measurement, in meters, and the wavelength of the side-band signal *i*, respectively. It must be noted that the expression above, φ_0 is provided in cycles. The meta-signal sub-carrier-phase estimation is performed by applying the wide-lane combination of the processed side-band carrier-phase observations,

$$\Phi_{sub} = \frac{f_2\Phi_2 - f_1\Phi_1}{f_2 - f_1} \quad (2)$$

where f_i is the center frequency of the *i*-th side-band signal.

Finally, the pseudorange computation of the meta-signal can be approached by combining the pseudorange observations of each side-band signal. However, each pseudorange must be multiplied by a factor which depends on the side-band signal amplitude, A, and the slope α of its auto-correlation function (ACF). Taken this into consideration, the meta-signal pseudorange, ρ_0 can be computed by means of the following expression:

$$\rho_0 = \frac{\alpha_1 A_1}{\alpha_1 A_1 + \alpha_2 A_2}\rho_1 + \frac{\alpha_2 A_2}{\alpha_1 A_1 + \alpha_2 A_2}\rho_2 \quad (3)$$

Considering that the signals involved are the E5a and E5b signals, which present the same power allocation and the ACF slope, a simple average between the side-band signal pseudorange observations is applied to achieve the meta-signal pseudorange.

$$\rho_0 = \frac{1}{2}(\rho_1 + \rho_2) \quad (4)$$

The single point positioning (SPP) comparison between the described Galileo E5a+E5b meta-signal approach and the Galileo E5 AltBOC is also provided in [1]. In the next section, our advanced positing engine employed to enhance the meta-signal performance is described.

3. Kalman-Filter-based Meta-signal Positioning Engine

In the M-SiPE engine, as depicted in

Figure **1**, a closed-loop Kalman filter is employed. This filter utilizes code pseudorange and sub-carrier measurements obtained from a RINEX observation file at each epoch to update its state-vector. The resulting float solution from the filter state-vector is subsequently fed into a specialized LAMBDA ambiguity resolution block. This block carries out sub-carrier ambiguity resolution, generating a fixed solution that is conditionally utilized to update the estimated receiver position. Since the employed meta-signal observations can be seen as single-frequency approach, where in addition the ambiguities have to be solved, we applied the approach of using the between single satellite difference (BSSD). There, the satellite with the highest elevation is fixed as reference from which the BSSD of the other visible satellites can be estimated.

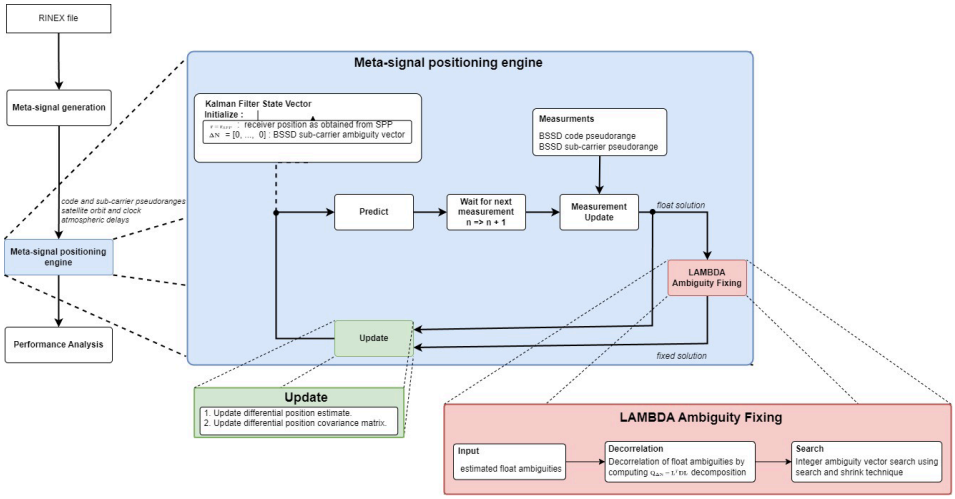

Figure 1. Meta-signal positioning engine (M-SiPE), adapted from [5]

The sub-carrier phase observations are inherently ambiguous, with an ambiguity, represented by integer multiples of the sub-carrier wavelength. This ambiguity is effectively resolved in the positioning domain through the LAMBDA ambiguity fixing method. In this study, we utilize the LAMBDA software package, originally developed at TU Delft [6], for implementation.

In the standard LAMBDA method implementation, float ambiguities are initially decorrelated using Cholesky decomposition and Z-transformation to reparametrize the float ambiguities vector and its covariance matrix. After the float ambiguity vector and covariance matrix are decorrelated, a mapping function is used to obtain the integer valued estimate. The integer estimate is determined through an integer search over a hyperellipsoid scaled by a constant and shaped by the ambiguities covariance matrix. Following completion of the search process, the fixed ambiguity vector is obtained by inverse Z-transform of the searched solution. Within this filter implementation, the back-

transformed integer candidate vectors are utilized for constructing the ambiguity fixing ratio and difference metrics. The ratio and difference are then compared against their respective thresholds. Whenever these thresholds are exceeded, a fixed solution update step is performed.

Considering correct resolution of these fixed ambiguities, the accuracy of the position error solution should be at the order of the sub-carrier measurement noise. Leveraging the low measurement noise associated with sub-carrier observations, substantial enhancement in position accuracy can be obtained.

4. Positioning Performance: Results and Analysis

4.1. Processing Toolchain

To formulate meta-signal measurements, pseudorange and carrier phase observations are obtained from a RINEX file, for both Galileo E5a and E5b, as described in section 2. In the second step the needed meta-signal observables, ρ_0 and φ_{sub} (in cycles) are computed, which are introduced later on to the M-SiPE which attempt to solve the sub-carrier ambiguities using the LAMBDA technique [6], where the associated MATLAB-based tool, as described in [7], has been appended to the KF-frame to decorrelate the estimated float BSSD-ambiguities. If this step can be conducted successfully, sub-decimeter level accuracy can be obtained. To achieve this level of accuracy various corrections, such as satellite orbits and atmospheric models, have to be considered when processing the observations. During the implementation and tuning of the M-SiPE, we figured out that the employed ionospheric model plays the key role in enabling robust fixing of the sub-carrier ambiguities from E5a-E5b sideband component. For this reason, we applied the Galileo single-frequency ionospheric correction algorithm (NeQuick G) which is realized by an official source code published by European Commission [8]. Figure 2 summarizes all above mentioned steps developed to combine both wide-lane technique and LAMBDA-method to provide reliable navigation information.

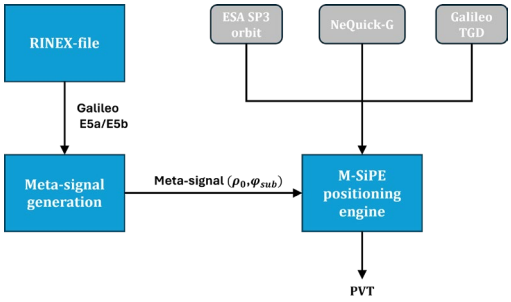

Figure 2. employed processing toolchain to evaluate meta-signal observations

4.2. Description of the Simulated Cases

In order to assess the robustness of the M-SiPE-tool against external signal impairments, such as multipath, various simulation scenarios have been generated. There, the multipath error is incorporated into the Galileo E5a and E5b pseudorange and carrier-phase, respectively, utilizing the following simplified model:

$$\delta\rho_{MP} = A\sin(2\pi f t) \quad (5)$$

where A is the amplitude of the signal and f is the frequency. In comparison to stochastic multipath models like [9] we find the use of this simpler deterministic model better to quantify the limit of multipath that the M-SiPE-tool can deal with by successfully resolving the ambiguity. The main simulation frame-work is realized on the RINEX-level, where a trajectory/static coordinate is given as ground-truth (see Figure 3) to build the GNSS observables for a specific GPS time, where the same error sources (ionospheric and tropospheric models) have been used as applied in the positioning. Before adding the

multipath signal, we assumed that the simulated observables are contaminated by only additive white Gaussian noise (AWGN).

In the simulations, this model was integrated into the signals starting from the 60th second onwards. The multipath model was chosen to be slow-varying, i.e. 0.01 Hz while the amplitude value was incrementally increased to examine the effects on the positioning solution. This was applied for both code and sub-carrier observations, separately. As highlighted by the blue boxes in the skyplot (see Figure 3), we contaminated 4 satellites from 11 visible Galileo satellites, i.e., E03, E05, E09 and E27, by multipath.

In general, the simulated scenarios can be spit into three main cases:

- In the first case (see Section 4.2.1), both code and sub-carrier observations were contaminated by this signal disturbance equally, where the amplitude values of 0.75 m, 1 m, 1.5 m, 1.75 m and 2 m were considered.
- In the second scenario block (see Section 4.2.1), the multipath amplitude in the sub-carrier signal was fixed to quarter of the wave length, while allowing the code values to be 2 m, 4 m, 8 m and 16 m.
- In the last test cases, zero code-multipath was set up while increasing the amplitude on the sub-carrier observations linearly, i.e. 0.24 m increments, until 2.4 m. On the other hand, the opposite strategy was applied to the code observations, where this time no multipath error was injected to the sub-carrier observation but the amplitude of the code-multipath was enlarged in 10 m steps until it attained 100 m amplitude. The results are summarized in Section 4.2.2.

Figure 3. Ground track of reference trajectory for the simulations. On the right side, the skyplot of the visible Galileo satellites is depicted, where the blue boxes indicate the contaminated satellites.

4.2.1. Simulation with Different Sub-carrier and Code Multipath Disturbance

In the figures, only the results with the minimum and the maximum employed multipath error, i.e. 0.75 m and 2 m (see general description in the previous paragraph) are visualized for the first simulation case. Beside the convergence time of the M-SiPE algorithm in the first 10 seconds where only the float solution is available, our technique is able to suppress the multipath effect applied on both meta-signal observables. This is especially true when the multipath error amplitude is negative, i.e. is going down to -0.75 m. However, when applying an amplitude of 2 m, the M-SiPE-tool seems to get some wrong fixed epochs at around 100 second. At the end of the scenario, between 140-150 seconds, the algorithm is able to recover and resolve the sub-carrier ambiguity term. In Figure 4 (b), it is also interesting to see a smooth transition between the float and fixing area.

The statistics, such as root mean square (RMS) of the position error, from the other scenarios with the values in-between, are summarized in Table 1-3. The associated five scenarios are indicated by the sub-script used to denote the different errors. In the tables, the error sub-script ranges from 1 to 9. The five cases just described are associated to sub-scripts from 1 to 5.

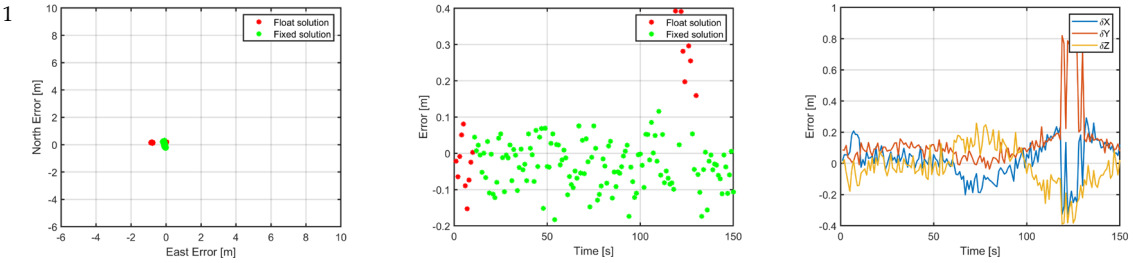

(**a**) (**b**) (**c**)

Figure 4. Positioning results with code and sub-carrier multipath amplitude of both equal to 0.75 m: (a) horizontal position error; (b) vertical position error; (c) position error in ECEF-frame.

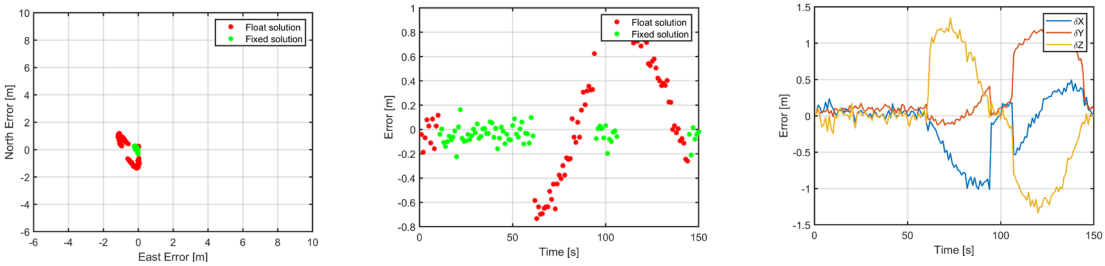

(**a**) (**b**) (**c**)

Figure 5. Positioning results with code and sub-carrier multipath amplitude of both equal to 2.00 m: (a) horizontal position error; (b) vertical position error; (c) position error in ECEF-frame.

In the remaining simulations numbered from 6 to 9 (see Table 1-3), the multipath amplitude of the sub-carrier-phase is fixed at 2.4 meters while the code values are 2 m, 4 m, 8 m and 16 m. The main reason for applying this constant multipath amplitude to the sub-carrier observations, is that multipath errors are limited by the quarter of the wavelength of the signal ($\delta\rho_{MP} \leq \frac{\lambda}{4}$) for carrier-phase observations [10]. In our case this corresponds to approximately 2.4 meters. Similar to the last 5 cases, only plots for two amplitude values, namely 2 and 16 m, are shown in Figure 6 and Figure 7. With the first test multipath amplitude, no significant change can be observed in comparison to Figure 4. But after applying higher multipath error, i.e. 16 m, the transition between float and fixed solution after activating the disturbance source at 60 sec, become somehow harsh (Figure 7.b). The oscillations of the sinusoidal signal can also be easily recognized in the north-east-plot (Figure 7.a). Therefore, the most significant error observed in the north direction (δN_9) where an RMS value of 2.57 m and maximum of 4.719 m (absolute value) has been achieved.

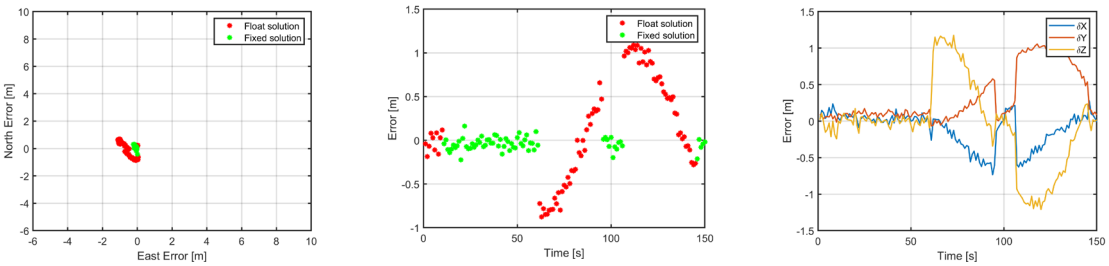

(**a**) (**b**) (**c**)

Figure 6. Positioning results with sub-carrier multipath amplitude of 2.40 m and code multipath amplitude of 2 m: (a) horizontal position error; (b) vertical position error; (c) position error in ECEF-frame.

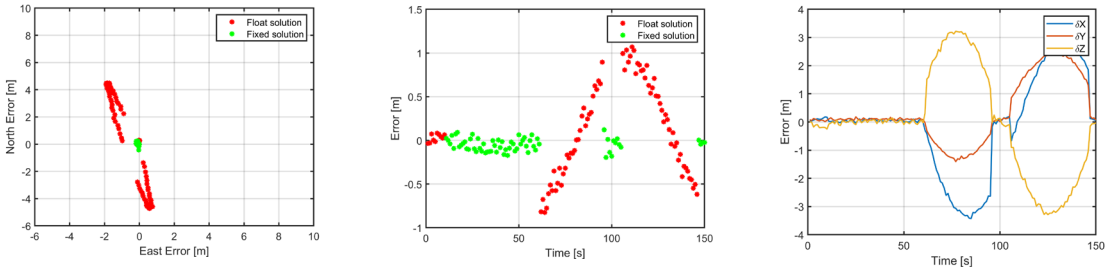

(**a**) (**b**) (**c**)

Figure 7. Positioning results with sub-carrier multipath amplitude of 2.40 m and code multipath amplitude of 16 m: (a) horizontal position error; (b) vertical position error; (c) position error in ECEF-frame.

Figure 8-10 summarize the statistics of all nine simulated scenarios graphically. In all these figures, it is shown that the impact of multipath on the positioning error exhibit a quadratic behavior, where the most affected axis is the north direction.

Table 1. Statistics for position error in east axis for all simulations.

East	Max [m]	Min [m]	RMS [m]
δE_1	0.040	-0.869	0.216
δE_2	0.053	-0.911	0.354
δE_3	0.014	-0.995	0.447
δE_4	0.034	-1.055	0.470
δE_5	0.070	-1.168	0.527
δE_6	0.061	-1.122	0.509
δE_7	0.141	-1.178	0.540
δE_8	0.290	-1.370	0.632
δE_9	0.761	-1.908	0.847

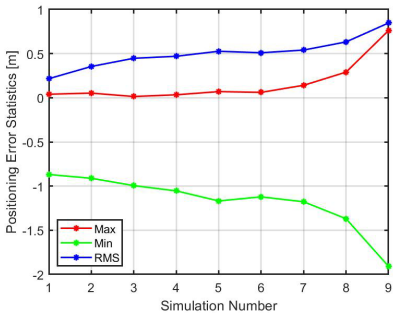

Figure 8. Statistics for positioning error in the east direction.

Table 2. Statistics for position error in north axis for all simulations.

North	Max [m]	Min [m]	RMS [m]
δN_1	0.326	-0.247	0.144
δN_2	0.295	-0.462	0.194
δN_3	0.470	-0.619	0.295
δN_4	0.572	-0.730	0.344
δN_5	1.188	-1.355	0.682
δN_6	0.683	-0.870	0.414
δN_7	1.187	-1.401	0.705
δN_8	2.298	-2.417	1.324
δN_9	4.488	-4.719	2.570

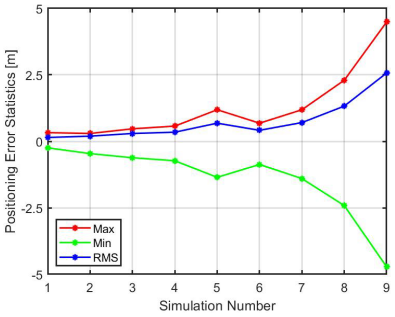

Figure 9. Statistics for positioning error in the north direction.

Table 3. Statistics for position error in up axis for all simulations.

Up	Max [m]	Min [m]	RMS [m]
δUp_1	0.392	-0.183	0.101
δUp_2	0.567	-0.394	0.168
δUp_3	0.766	-0.590	0.281
δUp_4	0.819	-0.687	0.330
δUp_5	0.924	-0.733	0.372
δUp_6	1.089	-0.876	0.453
δUp_7	1.134	-0.975	0.445
δUp_8	1.072	-0.801	0.433
δUp_9	1.071	-0.824	0.402

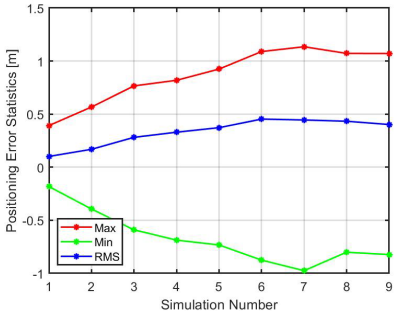

Figure 10. Statistics for positioning error in the up direction.

4.2.4. Impact of Linear Increasing Multipath Amplitude on Sub-carrier Ambiguity Fixing

Further examination of the multipath tolerance of the meta-signal is done by considering the effects of carrier and code multipath amplitude values separately. In the first set of simulations, the carrier amplitude is increased linearly from 0 to 2.4 m while keeping the code multipath to zero. Likewise, the second set of simulations are done by increasing the code multipath linearly from 0 to 100 m and zeroing the amplitude of multipath signal in the sub-carrier observations. In Figure 11, the results for fixing percentage as estimated by the M-SiPE-tool, i.e. the integrated LAMBDA technique, are shown. The x-axis shows an increasing amplitude in the multipath model while each data point shows one simulation setup, i.e. for each applied multipath amplitude.

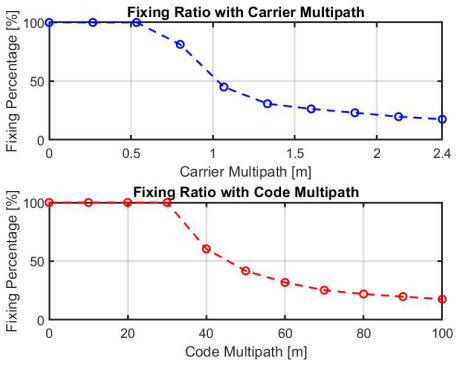

Figure 11. Fixing ratio with increasing carrier and code multipath amplitude.

The percentage of fixing is calculated over the duration of the multipath present instances of the simulation which starts from 60th second onwards. The multipath model is sinusoidal in nature (see Equation 5) and it reaches zero near 100th second. As a result, fixing is achieved in these instances and the fixing percentage reaches 17% when the multipath is at its highest. It was exapted, that such higher amplitude would deliver only float ambiguities, which is not the case here. The main reason for this behavior, is the employed simple multipath model, where the sine-wave increases to achieve the maximum and after that it goes towards its minimum point. When this error is near the zero-crossing area, the ambiguity fixing procedure is successful and position error is reduced. Alternatively, wrong fixing could also take place, which thereafter requires better tuning of the Kalman-filter, i.e. choose higher threshold to avoid it.

4. Conclusion and Outlook

In this contribution we demonstrated the potential of using meta-signal for positioning in harsh environments such as city urban canyons where signal reflection is inevitable. Thanks to the larger wave-length of the Galileo E5a-E5b sub-carrier signal, the employed LAMDA method allows to resolve the sub-carrier ambiguity term which leads to a greater accuracy in the range sub-decimeter, considering the single character of the used observables in the M-SiPE-tool. This accuracy would not be easy to achieve if the original observation, for example E5a/5b, were used. We observe that the multipath is no impact as long as the amplitude is less than 30 m (code) or 0.5 m (sub-carrier).

Future work may include more complex and realistic multipath simulation models such as the one described in [9]. Furthermore, the robustness and the benefit of the Beidou E1I-E1C meta-signal suggested in [11] can be explored and compared against the Galileo E5a-E5b case. It would be worthwhile, to adapt this technique to mass-market low-cost devices, such as smartphones, as recently some of them (for example Huawei P40 Pro [12]) provides already triple-frequency Beidou signal observations, including the E1I and E1C, which would allow much larger sub-carrier wave-length, i.e. 20.9 m than the one provided

by the E5a-E5b meta-signal. Unfortunately, only the Galileo E5a competent can be found in smartphone GNSS chips, thus potential of meta-signal with low-cost devices for the European satellite system cannot be currently exploited by using smartphones.

Author Contributions: Methodology, M.B., M.S.H. and M.A.; software, M.B. and M.S.H.; visualization, E. K.; writing—original draft, M.B.; writing—review and editing, M.B., E. K., M.S.H., M.A. and T.P.; supervision, T.P.; All authors have read and agreed to the published version of the manuscript.

Funding: This research was funded by the European Space Agency with ESA Contract No. 40001737747/22/NL/CRS (Architectures for Wide-Band Meta-Signal Processing in Low Cost Devices – HANDS CD).

Institutional Review Board Statement: Not applicable.

Informed Consent Statement: Not applicable.

Data Availability Statement: Data are available on request.

Conflicts of Interest: The authors declare no conflict of interest.

References

1. D. Borio und C. Gioia, „Reconstructing GNSS Meta-Signal Observations Using Sideband Measurements," NAVIGATION: Journal of the Institute of Navigation, Bd. 70, 2023.
2. D. Borio und C. Gioia, „GNSS Meta-signals, Dual-Frequency Combinations and the Double Phase Estimator," in Proceedings of the 2022 International Technical Meeting of The Institute of Navigation, 2022.
3. P. J. G. Teunissen, „Least-squares estimation of the integer GPS ambiguities," in Invited lecture, section IV theory and methodology, IAG general meeting, Beijing, China, 1993.
4. J. Wendel, F. M. Schubert und S. Hager, „A Robust Technique for Unambiguous BOC Tracking," NAVIGATION, Bd. 61, pp. 179-190, 2014.
5. M. S. Hameed, T. Woerz, T. Pany, J. Wendel, M. Paonni und T. Senni, „Demonstration of Meta-signal Positioning using LAMBDA Ambiguity Fixing Method within a Bit-true Simulation," in ION GNSS+, The International Technical Meeting of the Satellite Division of The Institute of Navigation, 2021.
6. P. J. G. Teunissen, „The least-squares ambiguity decorrelation adjustment: a method for fast GPS integer ambiguity estimation," Journal of geodesy, Bd. 70, p. 1–2, 1995.
7. M. Geodesy und D. U. o. T. Positioning, „LAMBDA software package : MATLAB implementation, Version 3.0".
8. European Commission, „Galileo Open Service Ionospheric Correction Algorithm for Galileo Single Frequency Receiver," 2016.
9. A. Lehner und A. Steingass, „A Novel Channel Model for Land Mobile Satellite Navigation," in Proceedings ION GNSS 2005, 2005.
10. P. J. G. Teunissen und O. Montenbruck, Hrsg., Springer Handbook of Global Navigation Satellite Systems, Cham, Switzerland: Springer, 2021.
11. D. Borio und C. Gioia, „Synthetic Meta-Signal Observations: The Beidou Case," Sensors, Bd. 24, p. 87, December 2023.
12. „HUAWEI P40 Pro - Specifications," Huawei Device Co., Ltd, 2024. [Online]. Available: https://consumer.huawei.com/en/phones/p40-pro/specs/. [accessed on 04 05 2024].

Disclaimer/Publisher's Note: The statements, opinions and data contained in all publications are solely those of the individual author(s) and contributor(s) and not of MDPI and/or the editor(s). MDPI and/or the editor(s) disclaim responsibility for any injury to people or property resulting from any ideas, methods, instructions or products referred to in the content.